CHEMISTRY OF MATERIALS

pubs.acs.org/cm

Article

Large Enhancement of Magnetocaloric and Barocaloric Effects by Hydrostatic Pressure in $La(Fe_{0.92}Co_{0.08})_{11.9}Si_{1.1}$ with a $NaZn_{13}$-Type Structure

Jiazheng Hao, Fengxia Hu,* Jian-Tao Wang, Fei-Ran Shen, Zibing Yu, Houbo Zhou, Hui Wu, Qingzhen Huang, Kaiming Qiao, Jing Wang,* Jun He, Lunhua He, Ji-Rong Sun, and Baogen Shen*

Cite This: *Chem. Mater.* 2020, 32, 1807−1818

Read Online

ACCESS | Metrics & More | Article Recommendations | Supporting Information

ABSTRACT: Solid-state refrigeration based on caloric effect has been regarded as an attractive alternative to the conventional gas compression technique. Boosting the caloric effect of a system to its optimum is a long-term pursuit. Here, we report enhanced magnetocaloric effect (MCE) and barocaloric effect (BCE) by hydrostatic pressure in $La(Fe_{0.92}Co_{0.08})_{11.9}Si_{1.1}$ with a $NaZn_{13}$-type structure. The entropy change ΔS_{MCE} is almost doubled under 11.31 kbar, while the ΔS_{BCE} is more than tripled under 9 kbar. To disclose the essence from the atomic level, neutron powder diffraction studies were performed. The results revealed that hydrostatic pressure sharpens the magnetoelastic transition and enlarges the volume change, $\Delta V/V$, during the transition through altering the intra-icosahedral Fe−Fe bonds rather than the inter-icosahedral distances in the $NaZn_{13}$-type structure. First-principles calculations were performed, which offers a theoretical support for the enlarged caloric effect related to the evolution of phase transition nature. Moreover, the enhanced lattice entropy change was calculated by Debye approximation, and a reliable way to evaluate BCE is demonstrated under a high pressure that DSC cannot reach. The present study proves that remarkable caloric effect enhancement can be achieved through tackling specific atomic environments by physical pressure, which may also be used to tailor other pressure-related effects, such as controllable negative thermal expansion.

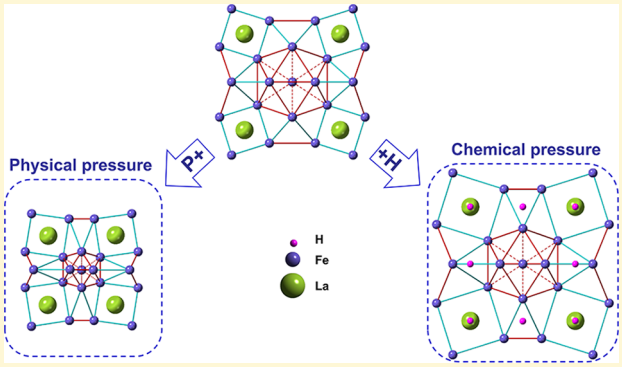

INTRODUCTION

Solid-state refrigeration based on caloric effect is of special interest since it is regarded as a promising, more efficient, and environmentally friendly alternative to gas compression-based refrigeration.[1−8] In recent years, considerable effort has been made in developing efficacious magnetic refrigerants, and one effective approach is to maximize the lattice contribution to the total entropy change under the moderate magnetic fields. Generally, for a magnetic material with magnetostructural/magnetoelastic transition, the total entropy change (ΔS_{Tot}) that characterizes caloric effect mainly consists of magnetic (ΔS_M) and lattice (ΔS_{Latt}) contributions, noting that the electronic entropy (ΔS_E) is negligibly small at a high temperature. The ΔS_M is theoretically limited by $\Delta S_M = R\ln(2J + 1)$, where J denotes the total angular momentum quantum number, while the ΔS_{Latt} is determined by the change of internal energy, which closely involves the volume change across phase transition.[9] Hence, maximizing the lattice contribution to total entropy change is an effective way to enhance the both MCE and BCE. For the magnetostructural/magnetoelastic phase transitions, pressure favors a small-volume phase, while magnetic field favors a ferromagnetic (FM) phase. External fields can shift the transition with respect to temperature. However, the magnitude of the volume change across the transitions, that is, the lattice contribution to the total entropy change (ΔS_{Tot}), usually remains constant or becomes smaller with external fields. For example, the lattice entropy change of $Gd_5Si_2Ge_2$, the milestone magnetocaloric material with magnetostructural transition,[10] is nearly independent of magnetic field, that is, $\Delta S_{Latt} \approx 9.9$ J kg^{-1} K^{-1}, while the spin contribution (ΔS_M) increases from 5.3 to 14.6 J kg^{-1} K^{-1} when the change of magnetic field increases from 0−2 to 0−10 T. A similar performance was observed for another composition of $Gd_5Si_{2.09}Ge_{1.91}$ where the ΔS_{Latt} also remains nearly constant, ∼9.2 Jkg^{-1} K^{-1}, while the ΔS_M increases from 4.7 to 9.0 J kg^{-1} K^{-1} with increasing the magnetic field change from 0-2 to 0-5 T.[11] For hexagonal MM′X compounds with magnetostructural transition, physical pressure can drive the transition occurring at a lower temperature with ΔS_{Tot} almost unchanged initially,[12] but the

Received: September 23, 2019
Revised: January 26, 2020
Published: January 27, 2020

transition becomes less abrupt, and both ΔS_{Tot} and ΔS_{Latt} quickly drop as the pressure reaches a critical value P = 3.7−6 kbar, depending on the compositions.[13] In other words, pressure- or magnetic field-induced increase of volume change $\Delta V/V$ and the resultant enhancement of ΔS_{Latt} were rarely observed.

It has been early discovered that $La(Fe,Si)_{13}$-based compounds show a great magnetocaloric effect (MCE), owing to the magnetoelastic transition and itinerant electron metamagnetic behavior.[7,14−18] In the cubic $NaZn_{13}$-type structure (space group: $Fm3c$, 112 atoms in a unit cell), Fe_1 and Fe_2 atoms occupy two distinct Wycko positions 8b and 96i, respectively, while La resides in 8a, and Si shares the 96i site with Fe_2. The Fe_1 and Fe_2 sites form an icosahedron, and Fe_1 at the center is surrounded by 12 Fe_2.[19−21] There are five kinds of Fe−Fe bonds, three of which (B1, B2, and B3) locate intra-icosahedron, while the other two (B4 and B5) locate inter-icosahedron (see the details in the main text, Figure 4a,b). $LaFe_{13-x}Si_x$ with a low Si content $1.0 < x < 1.6$ shows a first-order transition, and Curie temperature T_C locates around 200 K. Substitution of Fe by Co shifts the T_C to room temperature while weakening the first-order nature of transition.[7,18,22] As a result, the magnetic entropy change ΔS_{MCE} decreases, but it is still more than twice of that of the conventional refrigerant Gd.[23] Although a second-order-like transition appears for the Co-doped compounds, where both the magnetic and thermal hystereses approach zero, a considerable change of the isostructural volume, $-\Delta V/V \approx 1-1.4\%$, still exists, which promotes a large inverse barocaloric effect (BCE)[24] as well as a large magnetocaloric effect (MCE).[22]

Caloric effect driven by a hybrid field shows tremendous potential for both fundamental research and practical applications.[25−29] Our studies demonstrated that both MCE and BCE can be notably enhanced by hydrostatic pressure even for the Co-doped $LaFe_{13-x}Si_x$ with a second-order transition. We performed neutron powder diffraction (NPD) study on $La(Fe_{0.92}Co_{0.08})_{11.9}Si_{1.1}$ under a series of hydrostatic pressure. It is found that the application of pressure notably enlarges the negative volume expansion, $-\Delta V/V$, and sharpens the magnetoelastic transition through impacting the specific Fe−Fe bonds and spin fluctuations. Refinement results revealed that the intra-icosahedral B1, B2, and B3 bonds are mainly responsible for the enlargement and sharpness of negative volume expansion by pressure, while the inter-icosahedral B4 and B5 and the La−Fe bonds change a little. This result is distinct from the situation, introducing chemical pressure by H atoms in the $La(Fe,Si)_{13}$-based compounds where the enlarged lattice is mainly ascribed to the elongated B4 bond close to the 24d interstitial site occupied by H.[30] Such chemical pressure due to H atoms can also adjust the phase transition temperature in a wide temperature range through impacting the Fe−Fe bonds and interactions, but the sharpness of phase transition and the magnitude of MCE keep nearly unchanged with varying H contents.[14] To understand the underlined mechanism, first-principles calculations are performed, which supports the pressure-enhanced magneto-volume effect and the evolution from the second-order to the first-order transition in $La(Fe_{0.92}Co_{0.08})_{11.9}Si_{1.1}$. The enhanced lattice entropy change by pressure was quantitatively calculated by Debye approximation. The results prove that hydrostatic pressure is an effective means to sharpen phase transition and boost the lattice entropy change and hence enhance both MCE and BCE for the La−Fe−Co−Si magnetocaloric materials.

EXPERIMENTAL SECTION

Synthesis. The polycrystalline $La(Fe_{0.92}Co_{0.08})_{11.9}Si_{1.1}$ were prepared by arc melting constituent elements with purity better than 99.9 wt % under Ar protective atmosphere. Subsequently, the ingots were enveloped with a Ta foil and annealed in a sealed quartz tube with a high vacuum of 10^{-4} Pa for one month at 1353 K and then quenched in liquid nitrogen.

Characterization. High-resolution neutron powder diffraction (NPD) under in situ hydrostatic pressure was performed using a BT1 32-detector neutron powder diffractometer at the NIST Center for Neutron Research (NCNR). A Cu (311) monochromator was used to produce a monochromatic neutron beam with a wavelength of λ = 2.0775 Å. The sample was compressed in a pressure cell and the pressure was applied up to 9 kbar with helium gas as the pressure medium. Data were collected in the 2-theta range of 3−168° with a step size of 0.05°. All neutron diffraction patterns were refined using the GSAS/EXPGUI package.[31]

Magnetization measurements under hydrostatic pressures up to 11.31 kbar were performed in a nonmagnetic BeCu cylindrical pressure cell (Quantum Design) using a superconducting quantum interference device magnetometer (MPMS-7 T). Daphne 7373 oil was used as the liquid pressure-transmitting medium. The pressure in the BeCu cell was calibrated by measuring the shift of the superconducting transition temperature of Pb.

For calculating entropy change ΔS, "loop" modes were suggested to collect isothermal magnetization against magnetic field ($M-H$ curves), and then the calculated ΔS using the Maxwell relation can be reliable for first-order materials.[32−34] For $La(Fe,Si)_{13}$-based materials, we carefully investigated the ΔS by measuring the $M-H$ curves in both "loop" and "normal" modes, and found the ΔS based on the descending branch of $M-H$ curves in both modes are the same, even for $LaFe_{11.7}Si_{1.3}$ with strengthened first-order transition nature. So, in this work, the ΔS was obtained by adopting the descending branch of isothermal $M-H$ curves in normal mode. Here, the normal mode refers to collecting the isothermal $M-H$ curves continuously. The adopted loop mode includes the following steps: (i) cooling the sample in the maximum applied magnetic field to a temperature far below the transition temperature, (ii) heating in the maximum applied magnetic field up to the measuring temperature, and (iii) measuring the sample from the maximum applied magnetic field to zero. Then, repeat the above steps to measure the isothermal magnetization curve at the next higher temperature point.[33,34]

Heat flow measurements were carried out using a differential scanning calorimeter (Netzsch DSC 214). The ramping rate was 5 K min^{-1}. The total entropy at ambient pressure was obtained by recording heat flow out of/into the sample as a function of temperature after subtracting the baseline background.

First-principles calculations were performed using the Vienna ab initio simulation package (VASP)[35,36] with the projector augmented wave method[37,38] and spin-polarized generalized gradient approximation[39] for the exchange-correlation energy. The valence states $5s^25p^65d^16s^2$ for La, $3d^74s^1$ for Fe, $3d^84s^1$ for Co, and $3s^23p^2$ for Si were used with the energy cutoff of 500 eV for the plane wave basis set. To simulate the $La(Fe_{0.92}Co_{0.08)11.9}Si_{1.1}$ compound, a 2 × 2 × 2 supercell (including 8 atoms of La, 87 of Fe, 8 of Co, and 9 of Si) based on the $NaZn_{13}$ unit cell was adopted where the refined atomic positions and lattice parameters from NPD measurements under hydrostatic pressure were used. The Brillouin zone was sampled with a 2 × 2 × 2 Monkhorst-Pack special k-point grid. The energy convergence criterion was set at 10^{-6} eV throughout the present calculations.

RESULTS AND DISCUSSION

Temperature-dependent magnetization ($M-T$ curve) was measured on a $La(Fe_{0.92}Co_{0.08})_{11.9}Si_{1.1}$ compound under a

https://dx.doi.org/10.1021/acs.chemmater.9b03915
Chem. Mater. 2020, 32, 1807−1818

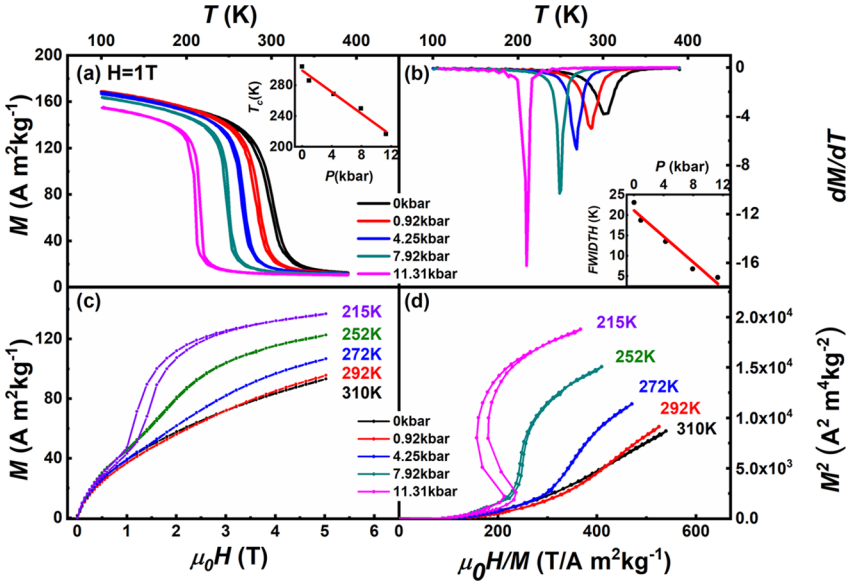

Figure 1. (a) Temperature-dependent magnetization of the $La(Fe_{0.92}Co_{0.08})_{11.9}Si_{1.1}$ compound on warming and cooling under various hydrostatic pressures with an external magnetic field H = 1 T applied. The inset shows the pressure dependence of Curie temperature, T_C, (b) $dM/dT-T$ curves deduced from panel (a) where the inset shows the pressure dependence of the full width at half maximum of dM/dT curves, (c) typical magnetic isothermals around T_C under different pressures, and (d) corresponding Arrott plots.

series of pressure on warming and cooling with a magnetic field of 1 T applied to demonstrate the impact of hydrostatic pressure on magnetic properties (Figure 1a). The sample undergoes a magnetic transition with Curie temperature, T_C, around ∼304 K in the absence of pressure, consistent with the previous report.[22] The value of T_C is determined by the minimum in the derivatives of $M-T$ curves. The application of hydrostatic pressure significantly sharpens the phase transition and shifts the T_C to a lower temperature at a rate of about $dT_C/dP = -7$ K kbar^{-1}. The T_C declines almost linearly from 304 to 217 K, as a pressure of 11.31 kbar was applied (see the inset of Figure 1a). To illustrate the gradual steepening of the transition under hydrostatic pressure, Figure 1b shows the derivative of magnetization, dM/dT, as a function of temperature under different pressures. The full width at half maximum narrows from 23.1 K at ambient pressure to 6.7 K under 11.31 kbar, while the maximum of dM/dT increases from 3.8 A m^2 kg^{-1} K^{-1} at ambient pressure to 16.3 A m^2 kg^{-1} K^{-1} under 11.31 kbar. These results quantify the steeper phase transition with increasing pressure. Figure 1c,d presents the typical magnetization isotherms ($M-H$) around T_C under different pressures and the corresponding Arrott plots (M^2-H/M), respectively. At ambient pressure, the $M-H$ curves show completely reversible behavior without magnetic hysteresis due to the nature of the second-order transition around T_C. With increasing hydrostatic pressure from 0 to 11.31 kbar, magnetic hysteresis gradually appears, and the slope of the Arrott plot develops from positive into negative, resulting in an S-shaped curve. These results signify the evolution of phase transition from the second order to first order according to the Landau phase transition theory,[40−42] which will lead to an enhanced magnetocaloric effect for $La(Fe_{0.92}Co_{0.08})_{11.9}Si_{1.1}$ compounds. More details about the electronic band structure calculations can be found in the following section.

Figure 2 displays the evaluated magnetic entropy changes, ΔS_{MCE}, based on the series of magnetic isothermal data using

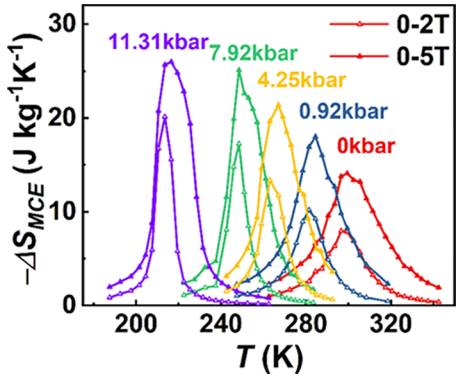

Figure 2. Entropy change for the magnetic field changes of 0−2 T and 0−5 T under different pressures for the $La(Fe_{0.92}Co_{0.08})_{11.9}Si_{1.1}$ compound.

Maxwell's relation $\Delta S_{MCE} = \int_0^H \left(\frac{\partial M}{\partial T}\right)_H dH$, which is the total entropy change contributed from both the spin and the lattice.[43,44] With the pressure raised to 11.31 kbar, the maximal $-\Delta S_{MCE}$ reaches ∼26.0 J kg^{-1} K^{-1} under 0−5 T, which is 1.8 times larger than the $-\Delta S_{MCE}$ (i.e., ∼14.1 J kg^{-1} K^{-1}) at ambient pressure. Moreover, the total area under the $\Delta S_{MCE}-T$ curve, which normally signifies refrigeration capacity (RC), increases from 542.0 J kg^{-1} at zero pressure to 615.3 J kg^{-1} under 11.31 kbar, equivalent to 13.5% improvement of RC. Both the enhanced ΔS_{MCE} and RC originates from the strengthened first-order transition. In particular, the enhanced lattice contribution by pressure plays a dominate role for the increased RC (see details in the following section).

For the first-order Co-free material $LaFe_{11.5}Si_{1.5}$, pressure-enhanced MCE has also been observed,[45] but the details involving lattice and atomic environments were not clear. To explore the origin of the pressure-enhanced MCE from the atomic level in the $La(Fe,Si)_{13}$-based materials, variable temperature neutron powder diffraction (NPD) under in situ

https://dx.doi.org/10.1021/acs.chemmater.9b03915
Chem. Mater. 2020, 32, 1807−1818

pressure (0, 3, 6, and 9 kbar) was performed on the Co-doped $La(Fe_{0.92}Co_{0.08})_{11.9}Si_{1.1}$ with a second-order transition. A representative neutron powder diffraction pattern collected at 300 K in the absence of pressure is given in Figure S1. Detailed refinement results of the variations of bond lengths, bond angles, and lattice parameters with temperature and pressure are summarized in Table S1 and Figures 3 and 4. As depicted

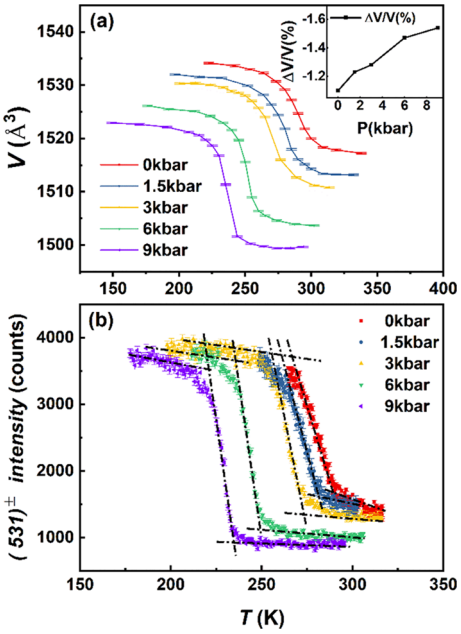

Figure 3. (a) Lattice volume as a function of temperature for the $La(Fe_{0.92}Co_{0.08})_{11.9}Si_{1.1}$ compound under different pressures. Inset shows the relative volume change $\Delta V/V$ as a function of pressure. (b) Neutron intensity (with error bars) of the (531) reflection as a function of temperature under different pressures.

in Figure 3a, a large negative lattice expansion, $\Delta V/V$, occurs along with the ferromagnetic ordering around the T_C. The $\Delta V/V$ is enlarged by 45% from −1.08 to −1.57% as the pressure increases from 0 to 9 kbar, and no saturation signs appear (inset of Figure 3a). Meanwhile, the phase transition becomes steeper with increasing pressure. Figure 3b shows the neutron intensity variations of the (531) reflection collected around T_C under different pressures, which further verifies the gradual steepening of the phase transition enforced by pressure. In contrast, the introduced chemical pressure by interstitial hydrogen atoms has almost no impact on the sharpness and the nature of phase transition,[14] and the entropy change keeps nearly unchanged with T_C shifting in a wide temperature range depending on H contents where H atoms occupy 24d interstitial sites and mainly affect the B4 Fe−Fe bonds inter-clusters.[30] The present study provides an approach to notably enhance the caloric effect, which may also be useful to achieve other pressure-related effects, such as controllable negative thermal expansion.

For the distinct effect caused by physical pressure, the variation of atomic local environments is the primary concern. Figure 4a is the schematic diagram of the partial lattice structure of $La(Fe,Si)_{13}$, showing 9 La atoms and four surrounding Fe-icosahedral clusters, and Figure 4b depicts the details around one Fe-icosahedron where all 5 Fe−Fe bonds and all related angles of Fe−Fe−Fe atomic chains are labeled. Figure 4c,d shows the refined Fe−Fe bond length

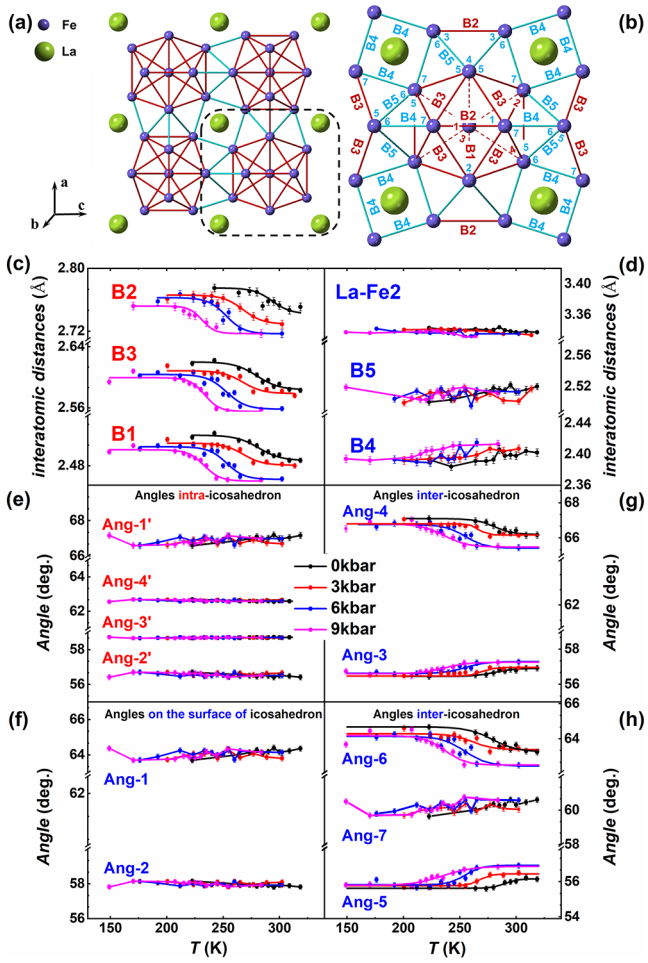

Figure 4. (a) Schematic diagram of the partial lattice structure of $La(Fe,Si)_{13}$ formed by 9 La atoms and four icosahedral clusters. (b) Schematic view of the five Fe−Fe bonds and all angles of Fe−Fe−Fe atomic chains, where the intra-icosahedral bonds (B1, B2, and B3) and angles (Ang-1′, Ang-2′, Ang-3′, and Ang-4′) are labeled by red, while the angles on the surface of the icosahedron (Ang-1 and Ang-2) and inter-icosahedral angles (Ang-3, Ang-4, Ang-5, Ang-6, and Ang-7) and bonds (B4 and B5) are all labeled by blue. The Fe−Fe interatomic distances in $La(Fe_{0.92}Co_{0.08})_{11.9}Si_{1.1}$ as a function of temperature under different pressures: (c) B1, B2 and B3, (d) B4, B5 and La-Fe_2. The bond angles of atomic chain as a function of temperature under different pressures. (e) Intra-icosahedral angles Ang-1′, Ang-2′, Ang-3′, and Ang-4′. (f) Angles on the surface of icosahedron Ang-1 and Ang-2. (g) Inter-icosahedral angles Ang-3 and Ang-4. (h) Inter-icosahedral angles Ang-5, Ang-6, and Ang-7.

intra-icosahedron (B1, B2, and B3) and inter-icosahedron (B4 and B5) as a function of temperature under different pressures, respectively. It can be noted that the intra-cluster bonds respond more sensitively to the temperature and show clear drops with increasing temperature around the T_C. Meanwhile, the B5 inter-cluster bonds remain nearly constant while the B4 inter-cluster bonds elongate slightly with increasing temperature noting that the B4 and B2 lie in one plane (Figure 4b). However, the variation magnitude of B4 (+0.87%, 0 kbar) is much less than those of the intra-cluster bonds (−1.21, −1.20, and − 1.28% for B1, B2, and B3, respectively). Hence, it can be concluded that the bonds within the icosahedron (B1, B2, and B3) mainly dominate the negative volume expansion ($\Delta V/V$) across T_C and the slope of phase transition. Meanwhile, the bond angles relax to counter the change of bond lengths and

https://dx.doi.org/10.1021/acs.chemmater.9b03915
Chem. Mater. 2020, 32, 1807−1818

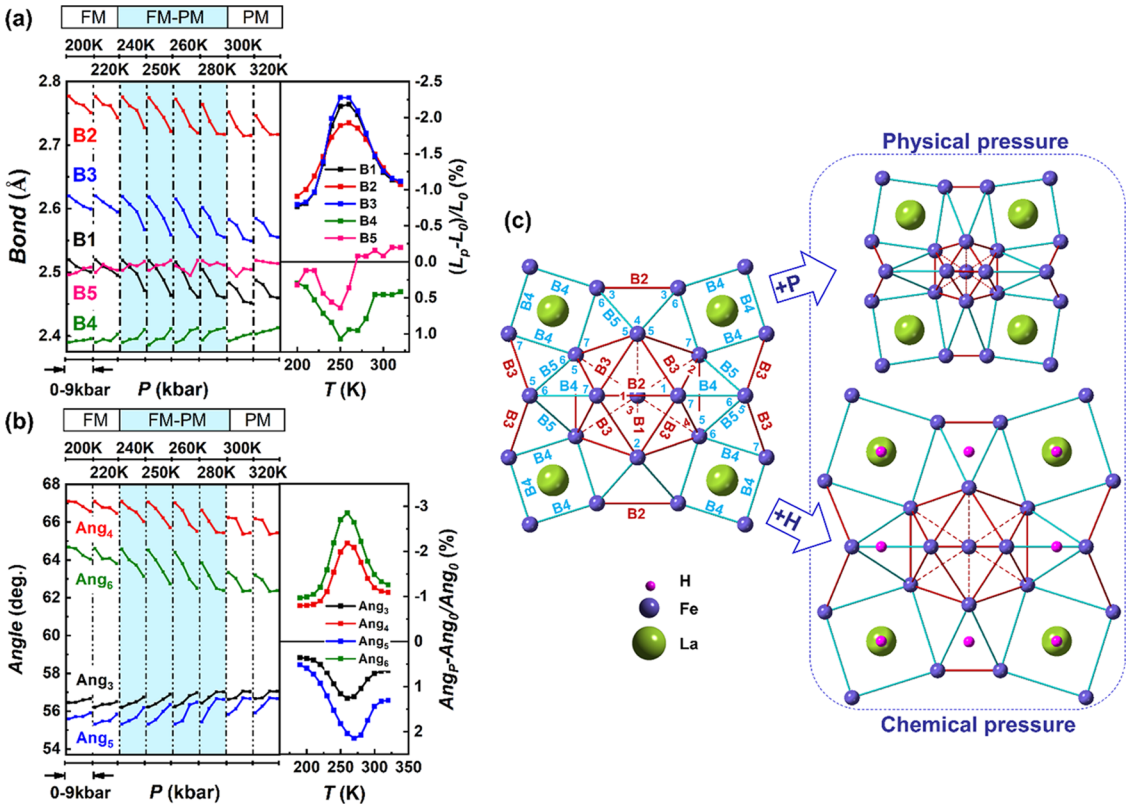

Figure 5. (a) Fe−Fe interatomic distances and (b) selected angles, Ang-3, Ang-4, Ang-5, and Ang-6 inter-icosahedrons in $La(Fe_{0.92}Co_{0.08})_{11.9}Si_{1.1}$ as a function of pressure at selected temperatures around T_C where the right panel of each displays the relative change under pressure from 0 to 9 kbar for the corresponding bonds and angles. (c) Schematic diagram indicating the variations of atomic local environments caused by physical pressure and chemical pressure.

maintain the lattice symmetry during phase transition. In the $NaZn_{13}$-type structure of $LaFe_{13}$ (see Figure 4b), there are four intra-icosahedral angles involving Fe1 atoms at the 8b site, which are labeled by red (Ang-1′, Ang-2′, Ang-3′, and Ang-4′), while two angles on the surface of the icosahedron (Ang-1 and Ang-2, labeled by blue) and five inter-icosahedral angles involving Fe2 atoms at the 96i site only (Ang-3, Ang-4, Ang-5, Ang-6, and Ang-7, labeled also by blue). The variations of these angles against temperature under different pressures are shown in Figure 4e−h. It can be seen that all four intra-icosahedral angles and the two angles on the surface of icosahedron show no anomaly and remain approximately unchanged around T_C (Figure 4e,f). These results strongly suggest that the symmetry of the icosahedron in the $NaZn_{13}$-structure keeps nearly independent of temperature and pressure, although the size of icosahedron shrinks under pressure (all the intra-icosahedral bonds B1, B2, and B3 shrink (Figure 4c)). In contrast, most inter-icosahedral angles change obviously with the ferromagnetic ordering. The Ang-4 and Ang-6, which face B2 and B3, respectively, become smaller along with the compression of B2 and B3, while both Ang-3 and Ang-5 enlarge and the Ang-7 remains almost constant to adapt the changes of Ang-4 and Ang-6 (Figure 4g,h).

To clearly illustrate the detailed responses of Fe−Fe bonds and the related angles to pressure, Figure 5a,b presents the pressure dependence of Fe−Fe bond lengths and angles, respectively, at several constant temperatures around T_C. All the intra-icosahedral bonds B1, B2, and B3 tend to contract as the pressure increases at any temperature, and the contraction becomes more rapid around T_C. In contrast, the inter-cluster bond B5 remains approximately constant, while the inter-cluster bond B4, the shortest one among the five Fe−Fe bonds, elongates slightly with increasing pressure. The right panel of Figure 5a shows the relative change of the corresponding bond length under pressure from 0 to 9 kbar. An extremum appears around T_C for all Fe−Fe bonds while trending oppositely for the intra-cluster (B1, B2, and B3) and inter-cluster (B4 and B5) bonds.

Moreover, the contraction of B1, B2, and B3 is more significant at the paramagnetic (PM) region above T_C compared to the FM region below T_C. The magnitude of the volume contraction by 9 kbar pressure around 320 K (−1.19%) is larger than that around 200 K (−0.80%) by 49% (Figure 3a). This behavior can be ascribed to the pronounced magnetoelastic softening despite the large volume decrease at the transition from the FM to the PM phase.[46,47] For $La(Fe,Si)_{13}$-based compounds, the combination of nuclear-resonant inelastic x-ray scattering (NRIXS) and density functional theory (DFT)-based first-principles calculations revealed that the PM phase is softer.[46,47] Therefore, the PM phase compresses more under pressure than the FM phase.

Accordingly, the inter-icosahedral bond angles Ang-4 and Ang-6 show similar dependence on temperature and pressure, noting that they face B2 and B3, respectively. Meanwhile, the inter-icosahedral Ang-3 and Ang-5 behave oppositely upon self-adjustment (Figure 5b). The right panel of Figure 5b shows the relative changes of these four angles under pressure from 0 to 9 kbar. An extremum also appears around T_C, but with opposite signs for the inter-icosahedral angles (Ang-4 and Ang-6) and (Ang-3 and Ang-5). Other angles on the surface of

https://dx.doi.org/10.1021/acs.chemmater.9b03915
Chem. Mater. 2020, 32, 1807−1818

and between the icosahedra keep almost independent of pressure (not shown).

All these details further prove that the symmetry of icosahedra in the $NaZn_{13}$-type structure remains unchanged and the lattice shrinkage caused by physical pressure is totally derived from the contraction of intra-cluster bonds (B1, B2, and B3), while the inter-cluster bonds (B4, B5) do not contribute at all. This is distinguishing from the source of lattice enlargement by introducing an interstitial hydrogen atom in the $La(Fe,Si)_{13}$-based compounds with the $NaZn_{13}$-type structure where the B4 bond close to the 24d interstitial site plays a dominate role, while the other four Fe−Fe bonds contribute little according to previous literatures.[30] Figure 5c shows the sketch, which elaborates the distinct effects of physical and chemical pressures on the lattice. Compared to the original (left panel), hydrostatic pressure shrinks the icosahedron, while the inter-icosahedral distances remain unchanged (the right upper panel), and the incorporation of interstitial H atoms at the 24d sites only elongates the inter-icosahedral B4 bonds, while barely affecting other intra-icosahedral bonds (the right lower panel). All these illustrate that the strengthened first-order nature of transition and the enlarged magnetovolume effect by physical pressure are closely relative to the compression of intra-icosahedral Fe−Fe bonds in the structure. In contrast, the reshaping of local environment around the 24d interstitial site by chemical pressure due to H atoms in the $NaZn_{13}$-type structure has almost no impact on the nature of transition and the magnetovolume effect, while the magnitude of entropy change keeps approximately constant with varying H contents even though the T_C shifts in a wide temperature range.[14] As for $LaFe_{1-x}Si_x$ without Co, the phase transition nature, T_C, and the volume change ($\Delta V/V$) across the T_C can be also continuously adjusted by tuning the Si content.[7] Our preliminary studies indicated that the change of atomic local environments with varying Si contents is different from the effect caused by hydrostatic pressure. The B1, B2, and B3 bonds of intra-icosahedron no longer change proportionally in one direction. The symmetry of icosahedron changes with varying Si contents because of the smaller radius of Si than Fe. Detailed studies are still under way. We hope to establish the relations between atomic environments and MCE for various cases (physical and chemical pressures).

For $La(Fe,Si)_{13}$-based compounds, the magnetovolume effect occurs along with the itinerant electronic metamagnetic (IEM) transition from the paramagnetic to the ferromagnetic state.[15,17,48] As a general feature of magnetovolume effect related to IEM transition, the reduction of spontaneous magnetization, M_s, caused by hydrostatic pressure is far smaller than its impact on Curie temperature T_C. For the present $La(Fe_{0.92}Co_{0.08})_{11.9}Si_{1.1}$ with second-order transition, ∼2% reduction of M_s was detected under 7.92 kbar, equivalent to $d\ln M_s/dP(1/GPa) \approx -0.025$, which is one order smaller than the effect of pressure on T_C with $d\ln T_C/dP(1/GPa) \approx -0.272$, noting the deduced $d\ln T_C/d\ln M_s \approx 10.9$. This behavior is very analogous to that in Fe−Pt invar-type alloys with strong magnetovolume effect and spin fluctuations.[49,50] The reduction of M_s is mainly caused by bandwidth narrowing due to the compressed volume under pressure, while the pressure-driven T_C strongly depends on magnetic free energy involving spin fluctuations. Through the magnetovolume effect, the applied pressure affects the renormalization effect related to spin fluctuations, hence largely shifts the T_C. The significant difference between the $d\ln M/dP$ and $d\ln T_C/d\ln M$ in the present $La(Fe_{0.92}Co_{0.08})_{11.9}Si_{1.1}$ implies a strong contribution from the renormalization effect of spin fluctuations.

For the electronic band structure possibly influenced by hydrostatic pressure, first-principles calculation using the fixed-spin-moment method was performed for $La(Fe_{0.92}Co_{0.08})_{11.9}Si_{1.1}$. Co and Si atoms are supposed to randomly occupy 96i sites together with Fe atoms in a 2 × 2 × 2 supercell of the $NaZn_{13}$ cell, which is composed of 8 atoms of La, 87 of Fe, 8 of Co, and 9 of Si, matching the $La(Fe_{0.92}Co_{0.08})_{11.9}Si_{1.1}$ composition. During calculation, atomic positions and lattice parameters adopt the data refined from the NPD patterns with and without pressure, so as to warrant that all the information of lattice change caused by pressure has been taken into account.

The calculated total and partial electronic density of states (DOS) are plotted in Figure S2. One can see that the spin-up and spin-down DOS peaks from −5 to 0 eV are mainly from the 3d bands of Fe and Co atoms. Moreover, there is a small splitting of 5d bands of La around the energy of −1.5 eV, indicating that the La-5d and (Fe,Co)-3d bands are well hybridized, but the main part of the partial DOS of the La-5d is located above the Fermi level. Meanwhile, the peaks from the 3s bands of Si are around the energy of −8 eV, lying far below E_F, and the peaks from the 4f bands of La are around the energy of 3 eV, above E_F. However, it is worth noting that calculations indicate that there is no obvious inconsistence between 0 and 9 kbar for the total electronic DOS curves in the ferromagnetic state, see details in Figure S3. This is consistent with macroscopic magnetic measurements, noting that the reduction of measured M_s under 7.92 kbar is as small as $d\ln M_s/dP(1/GPa) \approx -0.025$. In the majority spin band, the Fermi level E_F lies well-above the main part of the 3d density of state, suggesting that strong ferromagnetism keeps under both 0 and 9 kbar. While in the minority spin band, the E_F locates around the dip between the maxima around +2.0 eV and around −1.8 eV. A similar dip structure of DOS also appears in $LaFe_{11.5}Si_{1.5}$ and Fe−Pt, which was related to the small $d\ln M_S/dP$ and strong magnetovolume effect.[15,50]

However, the feature of nonmagnetic DOS is considered to be useful to discuss the order of FM−PM transition[15,51−54] for the materials with strong magnetovolume and spin fluctuations, such as Fe−Pt[50] and Fe−Ni[55] invar-type alloys. Figure 6 shows the DOS curves of the nonmagnetic state under

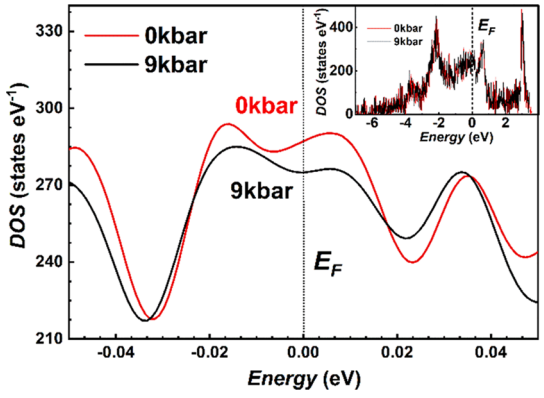

Figure 6. Details of total density of states near the Fermi level E_F of the $La(Fe_{0.92}Co_{0.08})_{11.9}Si_{1.1}$ compound in the nonmagnetic state under pressures of 0 and 9 kbar. The inset shows the total DOS in the nonmagnetic state. The Fermi energy is shifted to zero.

https://dx.doi.org/10.1021/acs.chemmater.9b03915
Chem. Mater. 2020, 32, 1807−1818

pressures 0 and 9 kbar for $La(Fe_{0.92}Co_{0.08})_{11.9}Si_{1.1}$. The common feature of the 3d DOS looks similar to that of fcc Fe, ordered Fe_3Pt, and Fe_3Ni.[50,55−57] A high DOS at the Fermi level E_F is considered to be a trigger of magnetic instability. The effect of pressure on the order of FM−PM transition can be expressed by the DOS behavior at the Fermi level E_F. In the following Landau−Ginzburg expansion including renormalization effect of spin fluctuations for free energy $F(M)$, the mode−mode coupling coefficient b determines the order of transition.[53,54]

$$F(M) = \frac{1}{2}aM(T)^2 + \frac{1}{4}bM(T)^4 + \frac{1}{6}cM(T)^6 + \cdots - HM \quad (1)$$

where the coefficients a, b, and c can be written in terms of the density of states and its derivatives with respect to the energy at the Fermi level. M denotes magnetization, and H denotes magnetic field. Especially, the mode−mode coupling coefficient b is expressed by the following equation,[51,52]

$$b = \frac{1}{16\rho(E_F)^3}\left\{\left(\frac{\rho(E_F)'}{\rho(E_F)}\right)^2 - \frac{\rho(E_F)''}{3\rho(E_F)}\right\} \quad (2)$$

where $\rho(E_F)$ represents the density of state (DOS) at the Fermi level E_F of the nonmagnetic state. The sign of b connects the order of transition, which is related to the curvature of DOS at the Fermi level.[51] Normally, a negative/positive b indicates first-order/second-order transition. In eq 1, order $F(M) = 0$, $H/M = a/2 + bM(T)^2/4 + cM(T)^4/6$, b is the slope of Arrott plots M^2-H/M. This is the reason why people usually characterize the order of transition by Arrott plots (see Figure 1d above). A change of DOS curvature caused by pressure can be clearly identified at the Fermi level, as shown in Figure 6. Based on eq 2, the calculated b appears to be $b = 1.76 \times 10^{-7}$ under $P = 0$, which turns to be $b = -5.4 \times 10^{-7}$ under $P = 9$ kbar. The sign of b changes from positive to negative, suggesting the pressure-driven evolution from second-order to first-order transition. These band structure calculations quantify the enhanced magnetovolume effect involving the first-order transition caused by hydrostatic pressure.

The enhanced magnetovolume effect by hydrostatic pressure will lead to increased magnetocaloric effect (MCE) and barocaloric effect (BCE). Generally, lattice entropy change (ΔS_{Latt}) plays a role as important as spin in the ferromagnetic materials undergoing concurrent lattice and magnetic transitions.[9,43] It is crucial to ascertain the individual contributions from spin and lattice. However, the lattice entropy change is usually difficult to measure. Early research[9] illustrated that the contribution of lattice entropy can be calculated from the MCE exhibited by closely related materials with and without first-order magnetic phase transition. Lately, Gschneidner et al. converged a collection of lattice contribution to the total entropy change for different materials undergoing first-order magnetic phase transition and found a linear functional relationship between the lattice entropy change and the lattice deformation ($\Delta V/V$), which is denoted by $\delta[\Delta V/V(\%)]/\delta[\Delta S_{Latt}] = 0.08(J\ kg^{-1}\ K^{-1})$.[9] However, it is known that this empirical relationship is a rough approximation ignoring the specific Grüneisen parameter and Debye temperature in different materials, which may affect the accurate evaluation of lattice entropy.

Based on Debye approximation, we quantitatively calculated the lattice entropy S_L of $La(Fe_{0.92}Co_{0.08})_{11.9}Si_{1.1}$ by the following equation,[43,58]

$$S_{Latt} = -3Nk_B \ln\left[1 - \exp\left(-\frac{\Theta}{T}\right)\right] + 12Nk_B\left(\frac{T}{\Theta}\right)^3 \int_0^{\Theta/T} \frac{x^3}{e^x - 1}dx \quad (3)$$

where N denotes the number of atoms per mole, k_B is the Boltzmann constant, and Θ is the Debye temperature, which can be determined by lattice vibration modes. For the deformed phase caused by phase transition, the Debye temperature Θ can be approximately expressed as follows,[43]

$$\Theta = \Theta_0(1 - \gamma\omega) \quad (4)$$

where Θ_0 denotes the Debye temperature in the absence of lattice deformation, γ is the Grüneisen parameter (generally γ has an absolute value between 1 and 3 for solid materials[59]), and ω is the volume change $\Delta V/V$ due to phase transition. For the $La(Fe_{0.92}Co_{0.08})_{11.9}Si_{1.1}$ compound, we derived the Θ_0 to be 330 K in the FM phase by linearly fitting the plot of C_p/T against T^2 in the low-temperature region below T_C according to the expression of specific heat capacity C_p for a metallic ferromagnet,[60−62]

$$C_p(T) = \alpha T + AT^3 \quad (5)$$

where the Sommerfeld coefficient α normally associates with the electronic specific heat, which is generally small ($b \approx 0.17$ mJ g^{-1} K^{-2}) and can be ignored.[61] $A = 12\pi^4R/(5\Theta_0{}^3)$, which is associated with the Debye temperature Θ_0.

Moreover, we can attain the Grüneisen parameter γ based on the Grüneisen law,[59] which can be approximately described as follows,

$$\alpha_v = (\gamma/k_0)(C_v/V_m) \quad (6)$$

where α_v is the volume thermal expansion coefficient, k_0 is the bulk modulus, C_v represents the isochoric specific heat per mole, and V_m is the molar volume. Here, the α_v is obtained from the refined data from NPD patterns, and the bulk modulus k_0 ($\sim 41.7 \times 10^9$ N m^{-2}) is derived from the measured Young's modulus and Poisson's ratio for LaFeCo-Si.[63,64] Based on eq 6, the Grüneisen parameter is obtained to be $\gamma = -2.4$ corresponding to the negative thermal expansion. As demonstrated by NPD data (see Table S1), the maximal volume changes ($\omega = \Delta V/V$) across phase transition under pressures 0, 3, 6, and 9 kbar is −1.08, −1.29, −1.50, and −1.57%, respectively. Furthermore, we can acquire the volume change ω at any temperature based on the refinement using NPD data by taking the onset of FM ordering as a reference, and then the Debye temperature Θ of the deformed phase can be deduced from eq 4. Accordingly, the lattice entropy S_{Latt} can be calculated based on eq 3 for various pressures, and the result is illustrated in Figure 7a. After deducting the contribution from the general anharmonic vibrations of atoms, the anomaly of lattice entropy $S_{Latt\text{-}PT}$ involving phase transition can be deduced (Figure 7b). Moreover, through comparing the $S_{Latt}-T$ curves with and without pressure ($S_{Latt\text{-}P}-S_{Latt\text{-}0}$, Figure 7a), the pressure-induced lattice entropy change ΔS_{Latt}, that is, the contribution of lattice entropy to the barocaloric effect ($\Delta S_{BCE\text{-}Latt}$), can be obtained, as shown in

https://dx.doi.org/10.1021/acs.chemmater.9b03915
Chem. Mater. 2020, 32, 1807−1818

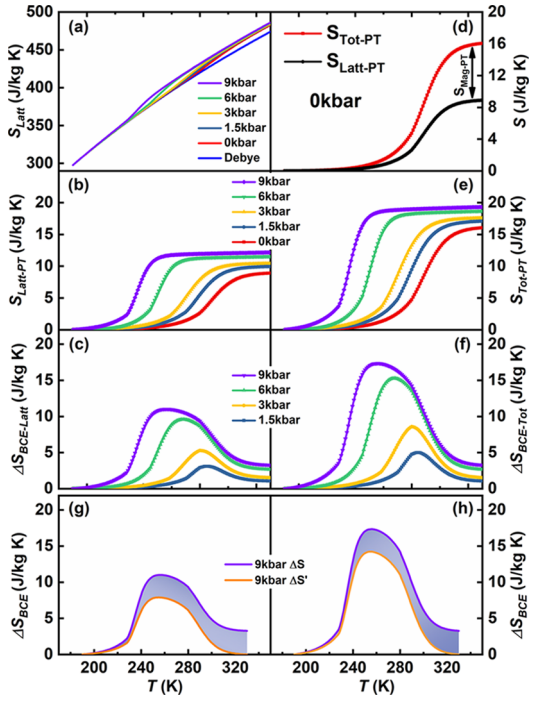

Figure 7. (a) Lattice entropy S_{Latt} as a function of temperature calculated by Debye approximation for the cases of various pressures where the blue line represents the lattice entropy ignoring phase transition. (b) Lattice entropy $S_{Latt\text{-}PT}$ involving phase transition only under different pressures. (c) Pressure-induced lattice entropy change $\Delta S_{BCE\text{-}Latt}$, that is, the lattice contribution to barocaloric effect. (d) Total entropy $S_{Tot\text{-}PT}$ measured by DSC, lattice entropy $S_{Latt\text{-}PT}$, and the spin entropy $S_{Mag\text{-}PT}$ involving phase transition at ambient pressure. (e) Total entropy $S_{Tot\text{-}PT}$ involving phase transition only under different pressures. (f) Pressure-induced total entropy change $\Delta S_{BCE\text{-}Tot}$, that is, barocaloric effect. (g) Comparison between $\Delta S_{BCE\text{-}Latt}$ and $\Delta S'_{BCE\text{-}Latt}$ without considering the effect of enlarged $\Delta V/V$ under 9 kbar. (h) Comparison of barocaloric effect between $\Delta S_{BCE\text{-}Tot}$ and $\Delta S'_{BCE\text{-}Tot}$ without considering the effect of enlarged $\Delta V/V$ under 9 kbar. The shaded area denotes the contribution from enlarged $\Delta V/V$ under 9 kbar.

Figure 7c. At ambient pressure, the thermal-induced ΔS_{Latt} during phase transition is 8.9 J kg^{-1} K^{-1}. It increases to 12.2 J kg^{-1} K^{-1} at 9 kbar, equivalent to a 37% growth (Figure 7b, Table 1). Meanwhile, the pressure-induced ΔS_{Latt} peaks around T_C and the maximum is about $\Delta S_{Latt} \approx 3.1$ J kg^{-1} K^{-1}for the pressure change from 0 to 1.5 kbar, and it rises more than three times up to 11.0 J kg^{-1} K^{-1} at 0−9 kbar (Figure 7c, Table 1).

La(Fe,Si)$_{13}$ materials undergo negative lattice expansion during the PM−FM transition on cooling. Landers et al. investigated the lattice vibrational entropy change ΔS_{Latt} in $LaFe_{11.6}Si_{1.4}$ by nuclear resonant inelastic X-ray scattering combined with density functional theory (DFT)-based first-principles calculations using the fixed-spin moment (FSM) approach.[46,47] The results demonstrated that the ΔS_{Latt} obtained by nuclear resonant inelastic X-ray scattering is a sizable quantity and contributes directly and cooperatively to the total entropy change ΔS at the phase transition. From the experimentally measured vibrational (phonon) density of states, VDOS, an abrupt increase (jump) in the Fe partial vibrational entropy ΔS_{Latt} was obtained on heating, and the increased magnitude of ΔS_{Latt} is substantial in comparison with the isothermal entropy change obtained using the Maxwell relation. Landers et al.[46,47] also compared the DFT-computed vibrational entropy change ΔS_{Latt} at a constant volume for the FM, PM, and FSM (fixed spin moment) states with the experimental results. Both the experimental and theoretical results demonstrated that an increase of the ΔS_{Latt} occurs with the FM-to-PM transition on heating. These results are consistent with our calculated lattice entropy by Debye approximation. The lattice entropy S_{Latt} shows a step increase around T_C with temperature increases.

Landers et al.[46] also calculated Debye temperatures Θ_D from the Lamb−Mössbauer factor based on the obtained VDOS for $LaFe_{11.6}Si_{1.4}$.[65] The obtained Θ_D drops by ∼4% from $\Theta_D \approx 363$ K in the FM phase to $\Theta_D \approx 348$ K in the PM phase. The trend of Θ_D with temperature is consistent with our calculated Θ_D by eq 4 (see Figure S5), though the absolute value of Θ_D is slightly different possibly due to the subtle differences of components. The Θ_D for $La(Fe_{0.92}Co_{0.08})_{11.9}Si_{1.1}$ drops by ∼3% from $\Theta_D \approx 300$ K (FM) to $\Theta_D \approx 292$ K (PM), which is comparable but somewhat smaller than the Θ_D drop of $LaFe_{11.6}Si_{1.4}$,[46] which is reasonable, considering the fact that the latter with first-order transition experiences a larger $\Delta V/V$ than the former. The decrease of Θ_D means the increase of lattice entropy S_{Latt}. These results further verify that the transition process from the large FM to the small PM phase is a process of increasing lattice entropy, the same as the the pure magnetic transition from the ordering (FM) to the disordering (PM) phase.

Moreover, it is well-accepted that the total entropy $S_{Tot\text{-}PT}$ involving phase transition can be reliably measured by calorimetric measurement using a differential scanning

Table 1. Results Based on Magnetic Measurements and on NPD[a]

based on magnetic measurements				based on NPD						
P [kbar]	ΔS_{MCE} (0−2 T) [J kg^{-1} K^{-1}]	ΔS_{MCE} (0−5 T) [J kg^{-1} K^{-1}]	total area [J kg^{-1}]	P [kbar]	$\Delta V/V$ [%]	$\Delta S_{Latt\text{-}ref}$ [J kg^{-1} K^{-1}]	$S_{Latt\text{-}PT}$ [J kg^{-1} K^{-1}]	$S_{Tot\text{-}PT}$ [J kg^{-1} K^{-1}]	$\Delta S_{BCE\text{-}Latt}$ [J kg^{-1} K^{-1}]	$\Delta S_{BCE\text{-}Tot}$ [J kg^{-1} K^{-1}]
0	−7.9	−14.1	542.0	0	−1.10	13.8	8.9	16.0		
0.92	−10.2	−18.0	539.8	1.5	−1.23	15.3	9.9	17.1	3.1	5.0
4.25	−13.4	−21.4	559.6	3	−1.28	15.9	10.4	17.6	5.3	8.6
7.92	−17.3	−25.1	569.8	6	−1.47	18.4	11.5	18.7	9.6	15.3
11.31	−20.1	−25.7	615.3	9	−1.54	19.3	12.2	19.3	11.0	17.4

[a]Based on magnetic measurements, the evaluated magnetic entropy change ΔS_{MCE} (0−2 T, 0−5 T) and the total areas under ΔS_{MCE}-T(0−5T) curves for different pressures. Based on lattice change ΔV/V refined from NPD, the estimated lattice entropy change $\Delta S_{Latt\text{-}ref}$ from its linear dependence on ΔV/V according to ref 9., the lattice entropy $S_{Latt\text{-}PT}$ involving phase transition from Debye approximation, and the deduced total entropy $S_{Tot\text{-}PT}$ involving phase transition, pressure-induced lattice entropy change $\Delta S_{BCE\text{-}Latt}$, and pressure-induced total entropy change $\Delta S_{BCE\text{-}Tot}$.

https://dx.doi.org/10.1021/acs.chemmater.9b03915
Chem. Mater. 2020, 32, 1807−1818

calorimeter (DSC).[13,66,67] $S_{Tot}(T) - S_{Tot}(T_0) = \int_{T_0}^{T} \frac{1}{T}\frac{\dot{Q}}{\dot{T}}dT$ where $\dot{Q}$ is the heat flow and $\dot{T}$ is the heating/cooling rate. We performed the calorimetric measurement by DSC (Netzsch DSC 214) with a temperature ramping rate of 5 K min^{-1}. The calculated total entropy $S_{Tot\text{-}PT}$ as a function of temperature at atmosphere pressure is shown in Figure 7d (red curve), where T_0 = 190 K at the FM state is taken as a reference and assuming $S_{Tot}(T_0 = 190\ K) = 0$. Note that the total entropy $S_{Tot\text{-}PT}$ mainly consists of contributions from spin and lattice. The deviation of $S_{Latt\text{-}PT}$ from $S_{Tot\text{-}PT}$ should express the contribution from spins in the ferromagnetic domains even without magnetic field applied (see Figure 7d). Moreover, it is reasonable to assume that the spin contribution to $S_{Tot\text{-}PT}$ remains nearly independent of pressure, noting that the spontaneous magnetization M_s reduces little ($d\ln M_s/dP(1/GPa) \approx -0.025$) even though the T_C largely shifts to a low temperature under pressure. This is the feature of IEM ferromagnetism with strong magnetovolume effect and spin fluctuations. Accordingly, the total $S_{Tot\text{-}PT}$ at different pressures can be obtained by summing the $S_{Latt\text{-}PT}$ (Figure 7b) and the contribution from spin ($S_{mag\text{-}PT}$, Figure 7d), as shown in Figure 7e. By comparing the $S_{Tot\text{-}PT}$–T curves with and without pressure (deducting $S_{Tot\text{-}PT\text{-}0}$ from $S_{Tot\text{-}PT\text{-}P}$, Figure 7e), pressure-induced total entropy change ΔS_{Tot}, that is, the barocaloric effect (BCE), can be deduced, as shown in Figure 7f. It is noticeable that the maximal BCE attains to $\Delta S_{BCE\text{-}Tot} \approx$ 17.4 J kg^{-1} K^{-1} for a pressure change of 0–9 kbar, which is more than three times larger compared to the one (~5.0 J kg^{-1} K^{-1}) at 0–1.5 kbar. These results are roughly consistent with the entropy change evaluated by DSC measurements with in situ pressure applied for a similar composition $LaFe_{11.33}Co_{0.47}Si_{1.2}$,[24] which has a lower T_C (~240 K) and a larger magnetovolume effect ($\Delta V/V \approx -1.5\%$) at atmosphere pressure compared to the present $La(Fe_{0.92}Co_{0.08})_{11.9}Si_{1.1}$ with $T_C \approx$ 304 K and $\Delta V/V \approx -1.1\%$ due to the different Co and Si stoichiometries. By normalizing the $\Delta S_{BCE\text{-}Tot}$ against the $\Delta V/V$ ($\Delta S_{BCE\text{-}Tot} \times (-1.5\%)/(-1.1\%)$), the $\Delta S_{BCE\text{-}Tot}$ for the present $La(Fe_{0.92}Co_{0.08})_{11.9}Si_{1.1}$ agrees well with that of $LaFe_{11.33}Co_{0.47}Si_{1.2}$[24] (see Figure 8). All these demonstrate that the estimated total entropy change under pressure up to 9 kbar, that is, BCE, is reliable. It is known that the applied in situ pressure in DSC is difficult to be as high as 9 kbar. The present work demonstrates a feasible way to assess BCE driven by high pressure based on NPD measurements.

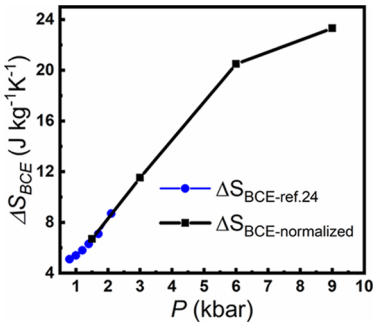

Figure 8. Pressure dependence of the maximum values of normalized barocaloric effect for the $La(Fe_{0.92}Co_{0.08})_{11.9}Si_{1.1}$ compound. The blue dots represent the maximum values of the barocaloric effect of $LaFe_{11.33}Co_{0.47}Si_{1.2}$ under different pressures in ref 24.

For comparison, we also evaluated the lattice entropy change $\Delta S_{Latt\text{-}ref}$ according to the empirical relationship $\delta[\Delta V/V(\%)]/\delta[\Delta S_{Latt}] = 0.08$(J kg^{-1} K^{-1}).[9] The result is given in Table 1. The $\Delta S_{Latt\text{-}ref}$ accounts for 86% of the total $\Delta S_{Tot\text{-}PT}$ measured by DSC at the ambient pressure, and grows to 100% at 9 kbar. Note that the contribution from the magnetic order during the phase transition cannot be absent although no magnetic field is applied, therefore the $\Delta S_{Latt\text{-}ref}$ is obviously overestimated where the specific Grüneisen parameter and Debye temperature in different materials were not taken into account. In other words, the lattice entropy change calculated by Debye approximation is more reliable.

The $La(Fe_{0.92}Co_{0.08})_{11.9}Si_{1.1}$ compound exhibits normal magnetocaloric effect (MCE) and inverse barocaloric effect (BCE), in both of which the lattice contribution plays an important role. Pressure-driven change of the electronic band structure and atomic local environments make the magnetic transition evolve from the second order to the first order. As a result, the ΔS_{MCE} peak grows sharper (Figure 2). The maximal ΔS_{MCE} under 11.31 kbar roughly doubled compared to that without pressure. More importantly, the area under the ΔS_{MCE} peak, which signifies the refrigeration capacity (RC), increases by 13.5% when a pressure of 9 kbar is applied (Table 1), which should totally originate from the enhanced lattice contribution by pressure. Simple calculations demonstrate that the area under the ΔS_{MCE} peak will keep unchanged if there is no volume change during the steepening process of phase transition driven by pressure. The negative lattice expansion around T_C is enlarged and does not show saturation with increasing pressure, hence the thermal-induced $\Delta S_{Tot\text{-}PT}$ grows with pressure. Calculations indicate that the thermal-induced lattice entropy change $\Delta S_{Latt\text{-}PT}$ accounts for 56% of total entropy $\Delta S_{Tot\text{-}PT}$ at atmospheric pressure (Figure 7d) during phase transition. This ratio increases to 63% as the pressure is up to 9 kbar (Figure 7b,e and Table 1) due to the enlarged $\Delta V/V$ by pressure (Figure 3a and its inset).

Moreover, we can quantitatively evaluate the contribution of enlarged $\Delta V/V$ to the notable enhancement of BCE by hydrostatic pressure. Due to the enhanced magnetovolume effect and the evolution of transition nature by pressure, barocaloric effect is also dramatically boosted with pressure. The maximal ΔS_{BCE} under 9 kbar grows by more than three factors. First, we assume that the effect of pressure on the movement and evolution of phase transition order remains unchanged without affecting the $\Delta V/V$. Then, the lattice entropy $S'_{Latt\text{-}PT}$ involving phase transition can also be obtained based on Debye approximation, as shown in Figure S4a. Similarly, we can get the pressure-induced lattice entropy change $\Delta S'_{Latt}$, that is, the contribution of the lattice entropy to the barocaloric effect ($\Delta S'_{BCE\text{-}Latt}$), as plotted in Figure S4b. Then, the total entropy $S'_{Tot\text{-}PT}$ involving phase transition (Figure S4c) as well as the pressure-induced total entropy change $\Delta S'_{BCE\text{-}Tot}$ (Figure S4d), that is, the barocaloric effect (BCE′) without considering the effect of enlarged $\Delta V/V$, can similarly be obtained, assuming that the spin contribution to the $S_{Tot\text{-}PT}$ remains nearly independent of pressure (Figure 7d). Figure 7g,h depicts the comparison between $\Delta S'_{BCE\text{-}Latt}$ and $\Delta S_{BCE\text{-}Latt}$, and between $\Delta S'_{BCE\text{-}Tot}$ and $\Delta S_{BCE\text{-}Tot}$, respectively, where the shaded area denotes the contribution from the enlarged $\Delta V/V$ under 9 kbar. It is evident that, compared to $\Delta S'_{BCE\text{-}Latt}$ and $\Delta S'_{BCE\text{-}Tot}$, the maxima of $\Delta S_{BCE\text{-}Latt}$ and $\Delta S_{BCE\text{-}Tot}$ curves increases by 39 and 22%, while the areas

https://dx.doi.org/10.1021/acs.chemmater.9b03915
Chem. Mater. 2020, 32, 1807–1818

under the curves, which connect RC enlarges by 47 and 20%, respectively, due to the enhanced contribution from the lattice.

CONCLUSIONS

In summary, large enhancement of MCE and BCE by hydrostatic pressure has been demonstrated in Co-doped $La(Fe,Si)_{13}$ with a second-order transition. The maximal ΔS_{MCE} almost doubled under 11.31 kbar compared to that without pressure, while the maximal ΔS_{BCE} under 9 kbar increases more than three times compared to that under 1.5 kbar. To understand the mechanism of such pressure-promoted MCE and BCE from the atomic level, NPD studies under a series of hydrostatic pressure were performed. Careful inspection of the refinement results indicate that the hydrostatic pressure enlarges the volume change, $\Delta V/V$, and sharpens the magnetoelastic transition through shortening the intra-icosahedral Fe−Fe bonds (B1, B2, and B3) rather than the inter-icosahedral bonds (B4 and B5) in the $NaZn_{13}$-type structure. This result is distinct from the situation of introducing chemical pressure by H atoms in the $La(Fe,Si)_{13}$-based compounds with $NaZn_{13}$-type structure where the enlarged lattice upon H absorption is mainly caused by the elongated B4 bond close to the 24d interstitial site. The introduced chemical pressure by H atoms in $La(Fe,Si)_{13}$-based compounds can adjust the phase transition temperature but not the sharpness of phase transition and the MCE. To understand the mechanism of the distinct effect by hydrostatic pressure, first-principles calculations are performed. The features of DOS in ferromagnetic and nonmagnetic states evidence the strong magnetovolume effect involving spin fluctuations and demonstrate the evolution of phase transition from second order to first order in nature, which is responsible for the enlarged caloric effect by hydrostatic pressure. Moreover, the contribution of enhanced lattice entropy change by pressure is quantitatively calculated by Debye approximation, and a reliable way to evaluate BCE is demonstrated under a high pressure that current DSC cannot reach. The present study provides an effective approach to achieve a significant enhancement of both MCE and BCE by utilizing specific atomic environments, which is also useful to achieve other related effects, such as controllable negative thermal expansion.

ASSOCIATED CONTENT

Supporting Information

The Supporting Information is available free of charge at https://pubs.acs.org/doi/10.1021/acs.chemmater.9b03915.

NPD pattern, crystal structure parameters, electronic DOS, and evaluation of the enlarged $\Delta V/V$ to the enhancement of BCE (PDF)

AUTHOR INFORMATION

Corresponding Authors

Fengxia Hu − *Beijing National Laboratory for Condensed Matter Physics & State Key Laboratory of Magnetism, Institute of Physics, Chinese Academy of Sciences, Beijing 100190, P. R. China; School of Physical Sciences, University of Chinese Academy of Sciences, Beijing 100049, P. R. China; Songshan Lake Materials Laboratory, Dongguan, Guangdong 523808, P. R. China*; Email: fxhu@iphy.ac.cn

Jing Wang − *Beijing National Laboratory for Condensed Matter Physics & State Key Laboratory of Magnetism, Institute of Physics, Chinese Academy of Sciences, Beijing 100190, P. R. China; School of Physical Sciences, University of Chinese Academy of Sciences, Beijing 100049, P. R. China; Fujian Innovation Academy, Chinese Academy of Sciences, Fuzhou, Fujian 350108, P. R. China*; orcid.org/0000-0001-5458-6711; Email: wangjing@iphy.ac.cn

Baogen Shen − *Beijing National Laboratory for Condensed Matter Physics & State Key Laboratory of Magnetism, Institute of Physics, Chinese Academy of Sciences, Beijing 100190, P. R. China; School of Physical Sciences, University of Chinese Academy of Sciences, Beijing 100049, P. R. China; Songshan Lake Materials Laboratory, Dongguan, Guangdong 523808, P. R. China*; Email: shenbg@iphy.ac.cn

Authors

Jiazheng Hao − *Beijing National Laboratory for Condensed Matter Physics & State Key Laboratory of Magnetism, Institute of Physics, Chinese Academy of Sciences, Beijing 100190, P. R. China; Division of Functional Material Research, Central Iron and Steel Research Institute, Beijing 100081, P. R. China*

Jian-Tao Wang − *Beijing National Laboratory for Condensed Matter Physics & State Key Laboratory of Magnetism, Institute of Physics, Chinese Academy of Sciences, Beijing 100190, P. R. China; School of Physical Sciences, University of Chinese Academy of Sciences, Beijing 100049, P. R. China; Songshan Lake Materials Laboratory, Dongguan, Guangdong 523808, P. R. China*; orcid.org/0000-0002-0786-1212

Fei-Ran Shen − *Beijing National Laboratory for Condensed Matter Physics & State Key Laboratory of Magnetism, Institute of Physics, Chinese Academy of Sciences, Beijing 100190, P. R. China; School of Physical Sciences, University of Chinese Academy of Sciences, Beijing 100049, P. R. China*

Zibing Yu − *Beijing National Laboratory for Condensed Matter Physics & State Key Laboratory of Magnetism, Institute of Physics, Chinese Academy of Sciences, Beijing 100190, P. R. China; School of Physical Sciences, University of Chinese Academy of Sciences, Beijing 100049, P. R. China*

Houbo Zhou − *Beijing National Laboratory for Condensed Matter Physics & State Key Laboratory of Magnetism, Institute of Physics, Chinese Academy of Sciences, Beijing 100190, P. R. China; School of Physical Sciences, University of Chinese Academy of Sciences, Beijing 100049, P. R. China*

Hui Wu − *NIST Center for Neutron Research, National Institute of Standards and Technology, Gaithersburg, Maryland 20899, United States*; orcid.org/0000-0003-0296-5204

Qingzhen Huang − *NIST Center for Neutron Research, National Institute of Standards and Technology, Gaithersburg, Maryland 20899, United States*

Kaiming Qiao − *Beijing National Laboratory for Condensed Matter Physics & State Key Laboratory of Magnetism, Institute of Physics, Chinese Academy of Sciences, Beijing 100190, P. R. China; School of Physical Sciences, University of Chinese Academy of Sciences, Beijing 100049, P. R. China*

Jun He − *Division of Functional Material Research, Central Iron and Steel Research Institute, Beijing 100081, P. R. China*

Lunhua He − *Beijing National Laboratory for Condensed Matter Physics & State Key Laboratory of Magnetism, Institute of Physics, Chinese Academy of Sciences, Beijing 100190, P. R. China; Songshan Lake Materials Laboratory, Dongguan, Guangdong 523808, P. R. China; China Spallation Neutron Source (CSNS), Guangdong 523808, P. R. China*

Ji-Rong Sun − *Beijing National Laboratory for Condensed Matter Physics & State Key Laboratory of Magnetism, Institute*

https://dx.doi.org/10.1021/acs.chemmater.9b03915
Chem. Mater. 2020, 32, 1807−1818

of Physics, Chinese Academy of Sciences, Beijing 100190, P. R. China; School of Physical Sciences, University of Chinese Academy of Sciences, Beijing 100049, P. R. China; Songshan Lake Materials Laboratory, Dongguan, Guangdong 523808, P. R. China; orcid.org/0000-0003-1238-8770

Complete contact information is available at: https://pubs.acs.org/10.1021/acs.chemmater.9b03915

Author Contributions

The manuscript was written through contributions of all authors.

Notes

The authors declare no competing financial interest.

■ ACKNOWLEDGMENTS

This work was supported by the National Key Research and Development Program of China (grant nos. 2017YFB0702702, 2019YFA0704904, 2018YFA0305704, 2017YFA0206300, 2017YFA0303601, and 2016YFB0700903), the National Natural Science Foundation of China (grant nos. 51531008, U1832219, 51771223, 51590880, 51971240, 11674378, 11934016, 11674364, and 11974387), and the Key Program and Strategic Priority Research Program (B) of the Chinese Academy of Sciences.

■ REFERENCES

(1) Pecharsky, V. K.; Gschneidner, K. A., Jr. Giant Magnetocaloric Effect in $Gd_5(Si_2Ge_2)$. *Phys. Rev. Lett.* **1997**, *78*, 4494.
(2) Neese, B.; Chu, B.; Lu, S. G.; Wang, Y.; Furman, E.; Zhang, Q. M. Large electrocaloric effect in ferroelectric polymers near room temperature. *Science* **2008**, *321*, 821−823.
(3) Tušek, J.; Engelbrecht, K.; Eriksen, D.; Dall'Olio, S.; Tušek, J.; Pryds, N. A regenerative elastocaloric heat pump. *Nat. Energy* **2016**, *1*, 16134.
(4) Mañosa, L.; Planes, A. Materials with Giant Mechanocaloric Effects: Cooling by Strength. *Adv. Mater.* **2017**, *29*, 1603607.
(5) Moya, X.; Kar-Narayan, S.; Mathur, N. D. Caloric materials near ferroic phase transitions. *Nat. Mater.* **2014**, *13*, 439−450.
(6) Tegus, O.; Brück, E.; Buschow, K. H. J.; de Boer, F. R. Transition-metal-based magnetic refrigerants for room-temperature applications. *Nature* **2002**, *415*, 150−152.
(7) Shen, B. G.; Sun, J. R.; Hu, F. X.; Zhang, H. W.; Cheng, Z. H. Recent Progress in Exploring Magnetocaloric Materials. *Adv. Mater.* **2009**, *21*, 4545−4564.
(8) Li, B.; Kawakita, Y.; Ohira-Kawamura, S.; Sugahara, T.; Wang, H.; Wang, J.; Chen, Y.; Kawaguchi, S. I.; Kawaguchi, S.; Ohara, K.; Li, K.; Yu, D.; Mole, R.; Hattori, T.; Kikuchi, T.; Yano, S. I.; Zhang, Z.; Zhang, Z.; Ren, W.; Lin, S.; Sakata, O.; Nakajima, K.; Zhang, Z. Colossal barocaloric effects in plastic crystals. *Nature* **2019**, *567*, 506−510.
(9) Gschneidner, K. A., Jr.; Mudryk, Y.; Pecharsky, V. K. On the nature of the magnetocaloric effect of the first-order magneto-structural transition. *Scr. Mater.* **2012**, *67*, 572−577.
(10) Pecharsky, V. K.; Gschneidner, K. A., Jr. Tunable magnetic regenerator alloys with a giant magnetocaloric effect for magnetic refrigeration from ∼20 to ∼290 K. *Appl. Phys. Lett.* **1997**, *70*, 3299−3301.
(11) Vitalij, K.; Pecharsky, A. O.; Gschneidner, K. A., Jr. Uncovering the structure−property relationships in $R_5(Si_xGe_{4-x})$ intermetallic phases. *J. Alloys Compd.* **2002**, *344*, 362−368.
(12) Caron, L.; Trung, N. T.; Brück, E. Pressure-tuned magneto-caloric effect in $Mn_{0.93}Cr_{0.07}CoGe$. *Phys. Rev. B* **2011**, *84*, No. 020414.
(13) Wu, R. R.; Bao, L. F.; Hu, F. X.; Wu, H.; Huang, Q. Z.; Wang, J.; Dong, X. L.; Li, G. N.; Sun, J. R.; Shen, F. R.; Zhao, T. Y.; Zheng, X. Q.; Wang, L. C.; Liu, Y.; Zuo, W. L.; Zhao, Y. Y.; Zhang, M.; Wang, X. C.; Jin, C. Q.; Rao, G. H.; Han, X. F.; Shen, B. G. Giant barocaloric effect in hexagonal Ni_2In-type Mn-Co-Ge-In compounds around room temperature. *Sci. Rep.* **2015**, *5*, 18027.
(14) Fujita, A.; Fujieda, S.; Hasegawa, Y.; Fukamichi, K. Itinerant-electron metamagnetic transition and large magnetocaloric effects in $La(Fe_xSi_{1-x})_{13}$ compounds and their hydrides. *Phys. Rev. B* **2003**, *67*, 104416.
(15) Fujita, A.; Fukamichi, K.; Wang, J. T.; Kawazoe, Y. Large magnetovolume effects and band structure of itinerant-electron metamagnetic $La(Fe_xSi_{1-x})_{13}$ compounds. *Phys. Rev. B* **2003**, *68*, 104431.
(16) Fujita, A.; Fujieda, S.; Fukamichi, K.; Mitamura, H.; Goto, T. Itinerant-electron metamagnetic transition and large magnetovolume effects in $La(Fe_xSi_{1-x})_{13}$ compounds. *Phys. Rev. B* **2001**, *65*, No. 014410.
(17) Hu, F. X.; Shen, B. G.; Sun, J. R.; Cheng, Z. H.; Rao, G. H.; Zhang, X. X. Influence of negative lattice expansion and metamagnetic transition on magnetic entropy change in the compound $LaFe_{11.4}Si_{1.6}$. *Appl. Phys. Lett.* **2001**, *78*, 3675−3677.
(18) Hu, F. X.; Shen, B. G.; Sun, J. R.; Wang, G. J.; Cheng, Z. H. Very large magnetic entropy change near room temperature in $LaFe_{11.2}Co_{0.7}Si_{1.1}$. *Appl. Phys. Lett.* **2002**, *80*, 826−828.
(19) Palstra, T. T. M.; Nieuwenhuys, G. J.; Mydosh, J. A.; Buschow, K. H. J. Mictomagnetic, ferromagnetic, and antiferromagnetic transitions in $La(Fe_xAl_{1-x})_{13}$ intermetallic compounds. *Phys. Rev. B* **1985**, *31*, 4622−4632.
(20) Palstra, T. T. M.; Mydosh, J. A.; Nieuwenhuys, G. J.; van der kraan, A. M.; Buschow, K. H. J. Study of the Critical-Behavior of the Magnetization and Electrical-Resistivity in Cubic $La(Fe, Si)_{13}$ Compounds. *J. Magn. Magn. Mater.* **1983**, *36*, 290−296.
(21) Wang, F.; Kurbakov, A.; Wang, G.-J.; Hu, F.-X.; Shen, B.-G.; Cheng, Z.-H. Strong interplay between structure and magnetism in $LaFe_{11.3}Co_{0.6}Si_{1.1}$: A neutron diffraction study. *Phys. B* **2006**, *385-386*, 343−345.
(22) Hu, F. X.; Gao, J.; Qian, X. L.; Ilyn, M.; Tishin, A. M.; Sun, J. R.; Shen, B. G. Magnetocaloric effect in itinerant electron metamagnetic systems $La(Fe_{1-x}Co_x)_{11.9}Si_{1.1}$. *J. Appl. Phys.* **2005**, *97*, 10M303.
(23) Brown, G. V. Magnetic heat pumping near room temperature. *J. Appl. Phys.* **1976**, *47*, 3673−3680.
(24) Mañosa, L.; González-Alonso, D.; Planes, A.; Barrio, M.; Tamarit, J. L.; Titov, I. S.; Acet, M.; Bhattacharyya, A.; Majumdar, S. Inverse barocaloric effect in the giant magnetocaloric La-Fe-Si-Co compound. *Nat. Commun.* **2011**, *2*, 595.
(25) Hou, H.; Finkel, P.; Staruch, M.; Cui, J.; Takeuchi, I. Ultra-low-field magneto-elastocaloric cooling in a multiferroic composite device. *Nat. Commun.* **2018**, *9*, 4075.
(26) Qu, Y. H.; Cong, D. Y.; Li, S. H.; Gui, W. Y.; Nie, Z. H.; Zhang, M. H.; Ren, Y.; Wang, Y. D. Simultaneously achieved large reversible elastocaloric and magnetocaloric effects and their coupling in a magnetic shape memory alloy. *Acta Mater.* **2018**, *151*, 41−55.
(27) Gong, Y. Y.; Wang, D. H.; Cao, Q. Q.; Liu, E. K.; Liu, J.; Du, Y. W. Electric field control of the magnetocaloric effect. *Adv. Mater.* **2015**, *27*, 801−805.
(28) Qiao, K.; Hu, F.; Liu, Y.; Li, J.; Kuang, H.; Zhang, H.; Liang, W.; Wang, J.; Sun, J.; Shen, B. Novel reduction of hysteresis loss controlled by strain memory effect in FeRh/PMN-PT heterostructures. *Nano Energy* **2019**, *59*, 285−294.
(29) Rocco, D. L.; de Campos, A.; Carvalho, A. M. G.; dos Santos, A. O.; da Silva, L. M.; Gama, S.; da Luz, M. S.; von Ranke, P.; de Oliveira, N. A.; Coelho, A. A.; Cardoso, L. P.; Souza, J. A. Influence of chemical doping and hydrostatic pressure on the magnetic properties of $Mn_{1-x}Fe_xAs$ magnetocaloric compounds. *Phys. Rev. B* **2016**, *93*, No. 054431.
(30) Jia, L.; Sun, J. R.; Shen, J.; Gao, B.; Zhao, T. Y.; Zhang, H. W.; Hu, F. X.; Shen, B. G. Influence of interstitial and substitutional atoms on the crystal structure of $La(Fe, Si)_{13}$. *J. Alloys Compd.* **2011**, *509*, 5804−5809.
(31) Toby, B. H. EXPGUI, a graphical user interface for GSAS. *J. Appl. Crystallogr.* **2001**, *34*, 210−213.

(32) Caron, L.; Ba Doan, N.; Ranno, L. On entropy change measurements around first order phase transitions in caloric materials. *J. Phys.: Condens. Matter* **2017**, *29*, No. 075401.
(33) Kaeswurm, B.; Franco, V.; Skokov, K. P.; Gutfleisch, O. Assessment of the magnetocaloric effect in La,Pr(Fe,Si) under cycling. *J. Magn. Magn. Mater.* **2016**, *406*, 259−265.
(34) Law, J. Y.; Franco, V.; Moreno-Ramírez, L. M.; Conde, A.; Karpenkov, D. Y.; Radulov, I.; Skokov, K. P.; Gutfleisch, O. A quantitative criterion for determining the order of magnetic phase transitions using the magnetocaloric effect. *Nat. Commun* **2018**, *9*, 2680.
(35) Sanyal, B.; Bose, S. K. Electronic structure and related thermal and magnetic properties of some ternary Invar alloys. *Phys. Rev. B* **2000**, *62*, 12730.
(36) Kresse, G.; Hafner, J. Ab initio molecular dynamics for liquid metals. *Phys. Rev. B* **1993**, *47*, 558−561.
(37) Blöchl, P. E. Projector augmented-wave method. *Phys. Rev. B* **1994**, *50*, 17953−17979.
(38) Kresse, G.; Joubert, D. From ultrasoft pseudopotentials to the projector augmented-wave method. *Phys. Rev. B* **1999**, *59*, 1758−1775.
(39) Perdew, J. P.; Burke, K.; Ernzerhof, M. Generalized gradient approximation made simple. *Phys. Rev. Lett.* **1996**, *77*, 3865−3868.
(40) Yamada, H. Metamagnetic transition and susceptibility maximum in an itinerant-electron system. *Phys. Rev. B* **1993**, *47*, 11211−11219.
(41) Carvalho, A. M. G.; Coelho, A. A.; Gama, S.; Gandra, F. C. G.; von Ranke, P. J.; de Oliveira, N. A. Investigation of the first-order metamagnetic transitions and the colossal magnetocaloric effect using a Landau expansion applied to MnAs compound. *Eur. Phys. J. B* **2009**, *68*, 67−72.
(42) Nishiyama, Y.; Hirooka, S. Itinerant-electron theory of metamagnetism. *Phys. Rev. B* **1997**, *56*, 7793−7795.
(43) Ranke, P. J. v.; de Oliveira, N. A.; Mello, C.; Carvalho, A. M. G.; Gama, S. Analytical model to understand the colossal magnetocaloric effect. *Phys. Rev. B* **2005**, *71*, No. 054410.
(44) Pecharsky, V. K.; Holm, A. P.; Gschneidner, K. A., Jr.; Rink, R. Massive magnetic-field-induced structural transformation in Gd_5Ge_4 and the nature of the giant magnetocaloric effect. *Phys. Rev. Lett.* **2003**, *91*, 197204.
(45) Jia, L.; Sun, J. R.; Shen, B. G.; Li, D. X.; Nimori, S. Effect of high pressure on the magnetocaloric property of $LaFe_{11.5}Si_{1.5}$. *J. Appl. Phys.* **2007**, *101*, 106108.
(46) Landers, J.; Salamon, S.; Keune, W.; Gruner, M. E.; Krautz, M.; Zhao, J.; Hu, M. Y.; Toellner, T. S.; Alp, E. E.; Gutfleisch, O.; Wende, H. Determining the vibrational entropy change in the giant magnetocaloric material $LaFe_{11.6}Si_{1.4}$ by nuclear resonant inelastic x-ray scattering. *Phys. Rev. B* **2018**, *98*, No. 024417.
(47) Gruner, M. E.; Keune, W.; Roldan Cuenya, B.; Weis, C.; Landers, J.; Makarov, S. I.; Klar, D.; Hu, M. Y.; Alp, E. E.; Zhao, J.; Krautz, M.; Gutfleisch, O.; Wende, H. Element-Resolved Thermodynamics of MagnetocaloricLa$Fe_{13-x}Si_x$. *Phys. Rev. Lett.* **2015**, *114*, No. 057202.
(48) Fujita, A.; Akamatsu, Y.; Fukamichi, K. Itinerant electron metamagnetic transition in $La(Fe_xSi_{1-x})_{13}$ intermetallic compounds. *J. Appl. Phys.* **1999**, *85*, 4756−4758.
(49) Moruzzi, V. L. Singular volume dependence of transition-metal magnetism. *Phys. Rev. Lett.* **1986**, *57*, 2211−2214.
(50) Podgórny, M. Electronic structure of the ordered phases of Pt-Fe alloys. *Phys. Rev. B* **1991**, *43*, 11300−11318.
(51) Shimizu, M.; Inoue, J. Thermal Spontaneous Ferromagnetism in Y_2Ni_7 Intermetallic Compound. *J. Phys. F: Met. Phys.* **1987**, *17*, 1221−1229.
(52) Moriya, T. On the Possible Mechanisms for Temperature-Induced Ferromagnetism. *J. Phys. Soc. Jpn.* **1986**, *55*, 357−366.
(53) Yamada, H. Pressure Effect in an Itinerant-Electron Metamagnet at Finite-Temperature. *J. Magn. Magn. Mater.* **1995**, *139*, 162−170.
(54) Yamada, H.; Goto, T. Itinerant-electron metamagnetism and giant magnetocaloric effect. *Phys. Rev. B* **2003**, *68*, 184417.
(55) Entel, P.; Hoffmann, E.; Mohn, P.; Schwarz, K.; Moruzzi, V. L. First-principles calculations of the instability leading to the Invar effect. *Phys. Rev. B* **1993**, *47*, 8706−8720.
(56) Moruzzi, V. L.; Marcus, P. M.; Schwarz, K.; Mohn, P. Ferromagnetic phases of bcc and fcc Fe, Co, and Ni. *Phys. Rev. B* **1986**, *34*, 1784−1791.
(57) Maosa, L.; Saunders, G. A.; Rahdi, H.; Kawald, U.; Pelzl, J.; Bach, H. Acoustic-mode vibrational anharmonicity related to the anomalous thermal expansion of Invar iron alloys. *Phys. Rev. B* **1992**, *45*, 2224−2236.
(58) Bean, C. P.; Rodbell, D. S. Magnetic Disorder as a First-Order Phase Transformation. *Phys. Rev.* **1962**, *126*, 104−115.
(59) Slack, G. A. The Thermal Conductivity of Nonmetallic Crystals. In *Solid State Phys*; Ehrenreich, H.; Seitz, F.; Turnbull, D. Eds. Academic Press: 1979, *34*, pp 1−71.
(60) Reddy, P. J. Calculation of the debye temperatures of crystals. *Physica* **1963**, *29*, 63−66.
(61) Lovell, E.; Ghivelder, L.; Nicotina, A.; Turcaud, J.; Bratko, M.; Caplin, A. D.; Basso, V.; Barcza, A.; Katter, M.; Cohen, L. F. Low-temperature specific heat in hydrogenated and Mn-doped La(Fe, $Si)_{13}$. *Phys. Rev. B* **2016**, *94*, 134405.
(62) Reifenberg, J. P.; Panzer, M. A.; Kim, S.; Gibby, A. M.; Zhang, Y.; Wong, S.; Wong, H. S. P.; Pop, E.; Goodson, K. E. Thickness and stoichiometry dependence of the thermal conductivity of GeSbTe films. *Appl. Phys. Lett.* **2007**, *91*, 111904.
(63) Kaeswurm, B.; Barcza, A.; Vögler, M.; Geiger, P. T.; Katter, M.; Gutfleisch, O.; Cohen, L. F. Behaviour of the Young's modulus at the magnetocaloric transition in $La(Fe,Co,Si)_{13}$. *J. Alloys Compd.* **2017**, *697*, 427−433.
(64) Huang, D.; Kou, R.; Gao, J.; Haglund, A.; Yan, J.; Keppens, V.; Mandrus, D.; Ren, Y. Influence of Co-doping on the Crystal Structure, Magnetocaloric Properties and Elastic Moduli of the La(Fe, $Si)_{13}$ Compound. *TMS 2018 147th Annual Meeting & Exhibition Supplemental Proceedings* 2018, 181−190, DOI: 10.1007/978-3-319-72526-0_17.
(65) Rosén, J.; Grimvall, G. Anharmonic lattice vibrations in simple metals. *Phys. Rev. B* **1983**, *27*, 7199−7208.
(66) Mañosa, L.; González-Alonso, D.; Planes, A.; Bonnot, E.; Barrio, M.; Tamarit, J.-L.; Aksoy, S.; Acet, M. Giant solid state barocaloric effect in the Ni-Mn-In magnetic shape-memory alloy. *Nat. Mater.* **2010**, *9*, 478−481.
(67) Vallone, S. P.; Tantillo, A. N.; Dos Santos, A. M.; Molaison, J. J.; Kulmaczewski, R.; Chapoy, A.; Ahmadi, P.; Halcrow, M. A.; Sandeman, K. G. Giant Barocaloric Effect at the Spin Crossover Transition of a Molecular Crystal. *Adv. Mater.* **2019**, *31*, 1807334.

https://dx.doi.org/10.1021/acs.chemmater.9b03915
Chem. Mater. 2020, 32, 1807−1818